Chapter 9
Tool-Tip Vibration at High Frequencies

Abstract This chapter presents a theoretical and experimental investigation of the influence of tool-tip vibration on surface generation in single-point diamond turning. Although it is well known that the relative vibration between the tool and the workpiece plays an important role in surface generation in single-point diamond turning, most of the previous work has focused on studying the relative tool-work vibration in the infeed (thrust force) direction while the significant contribution of the effect of the tool-tip vibration in the cutting force direction has been overlooked. In ultraprecision diamond turning, the characteristic twin peaks are identified and found to correspond to the tool-tip vibrations by power spectrum density analyses. The vibrations possess the features of small amplitude but high frequency. A theoretical physical model is proposed to describe and correlate the characteristic peaks in the frequency domain with the behaviour of the tool-tip vibration in the steady-state cutting process. The proposed model has the capability of capturing the dominant factors influencing the surface roughness of the machined surfaces.

9.1 Identification of Tool-Tip Vibration by Power Spectrum Analysis

A series of cutting experiments have been conducted on a two-axis ultraprecision lathe machine (Optoform 30 from Rank Pneumo from USA). A Kistler 9252A force transducer is mounted between the tool shank and the holder with a pre-loading force. The three-axis signals of forces are recorded during steady-state cutting with a Tektronix TDS 744A digitising oscilloscope. The equipment setup is shown in Fig. 9.1. The background information of the signal of cutting force is first collected and studied in the air-cutting experiments. The signals are recorded before and after running the spindle, under different conditions with and without coolant mist. The turning experiments are then conducted with different non-ferrous work materials, including pure copper, aluminium alloy 6061 and brass. The spindle speed is set at 5000 rpm, depth of cut at 10 μm and feed rate at 20 mm/min. A diamond cutting tool with a nose radius of 1.49 mm is used. The sampling frequency is set at

S.S. To et al., *Materials Characterisation and Mechanism of Micro-Cutting in Ultra-Precision Diamond Turning*, DOI 10.1007/978-3-662-54823-3_9

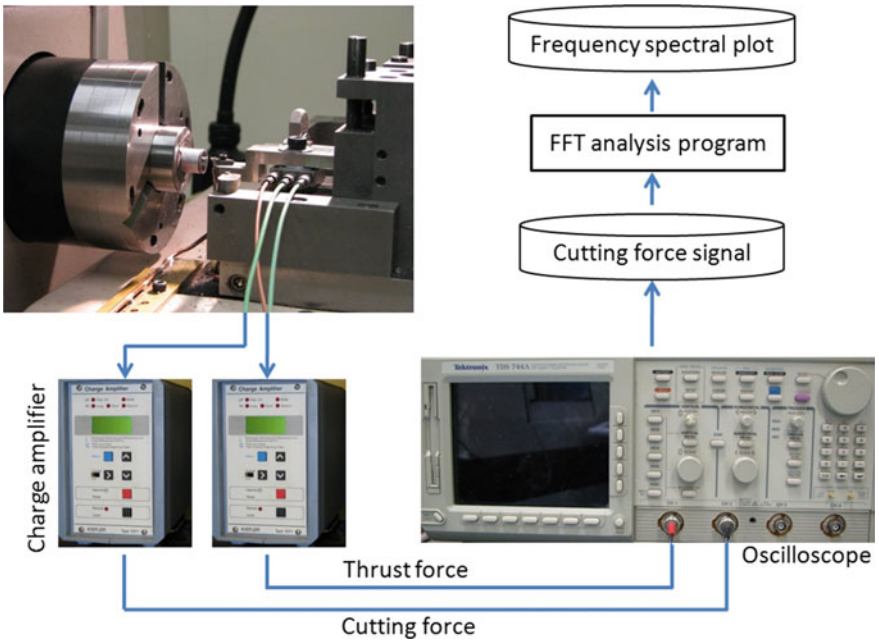

Fig. 9.1 Equipment setup for the analysis of the signals of cutting force

50 kHz. Thus, the frequencies below 25 kHz can be accurately calculated in the power spectrum analysis with regard to the Nyquist limit. The signals obtained in the time domain are transformed to the frequency domain by Fast Fourier transform (FFT). Power spectrum density (PSD) analysis is performed based on the output of FFT transform.

For the purpose of comparison and identification of the process damping effect induced by the elastic recovery on the clearance face of cutting tool, no coolant mist or lubricant is used in the cutting tests, so that no further damping factors, such as fluid damping, are introduced into the dynamic system of the tool tip and work materials. However, the coolant mist is employed again to establish a correlation between the characteristic twin peaks of tool-tip vibration and the surface roughness in the experiments in the subsequent sections of this chapter. In a control experiment, which aims at eliminating the effect of process damping, bakelite is selected as the work material. With its brittle nature, bakelite can provide the external excitation to the tool tip without introducing new damping factors into the system.

In order to visualise the effect of tool-tip vibration on the surface finish, a micro-cutting test is conducted without overlapping of the cutting marks. Thus, a diamond-turned mark is cut with zero-feed velocity and spindle speed of 2000 rpm on a preformed aluminium alloy Al6061 workpiece. The depth of cut is set to 10 μm in the zero-feed experiment. The surface is then examined by an optical microscope Olympus BX60.

The experimental power spectrum density plots of the cutting force signals recorded in the air-cutting tests under different conditions are shown in Fig. 9.2. It is observed that the characteristic twin peaks appear at a frequency around 13 and 14 kHz in Fig. 9.2a, c, while in Fig. 9.2b, d, the twin peaks disappear due to the absence of the excitation on the tool tip by the coolant mist. Furthermore, Fig. 9.2b, d indicate that the rotation of the spindle does not affect the twin peaks except for the introduction of some background information in the frequency domain. Figure 9.2e, f, g reveal that the characteristic twin peaks exist in the cutting of ductile non-ferrous materials due to the induced excitation of the tool tip. It is obvious that the frequencies of the twin peaks stay unchanged with different work materials, however, the relative amplitude of the twin peaks is of interest in the following sections. The right peak (around 14 kHz) is regarded as the excited natural frequency induced by the micro-cutting process, while the left peak (around 13 kHz) is generated due to the process damping effect caused by the interaction between the tool tip and the elastic recovery induced ploughing force between the diamond-turned surface and the clearance face of the cutting tool. It is interesting to note that different mechanical properties of the work materials, such as Young's modulus, yield stress, hardness and friction coefficient, lead to different extents of such process damping effects. However, due to the brittle nature of bakelite, the elastic recovery induced ploughing force is negligible, i.e. the process damping can barely be observed in the bakelite micro-cutting process. This agrees with our experimental observation. The left peak of the characteristic twin peaks does not exist in Fig. 9.2h.

According to the turned surface in Fig. 9.3, the distance (d) between two adjacent bar-shape marks can be calculated with the help of the non-contact optical profiler Wyko NT8000. The average distance is calculated to be around 73.7 μm. Thus, the frequency of the periodic characteristic marks is estimated to be around 14.1 kHz in Eq. (9.1), which is consistent with the above-mentioned frequencies obtained from the cutting force signals. The natural frequencies of the characteristic twin peaks (the right peak) result in the appearance of the bar-shape marks on the single turning mark.

$$f_{\text{calc}} = \frac{2\pi R \times \text{spindle}/60\ \text{s}}{d} = \frac{2\pi \times 5\ \text{mm} \times 2000\ \text{rpm}/60\ \text{s}}{0.0737} \approx 14.1\ \text{kHz} \quad (9.1)$$

9.2 Characteristic Twin Peaks and Material Properties

Micro-cutting trials have been conducted to reveal the correlation between the characteristic twin peaks of high-frequency tool-tip vibration and material properties. Aluminium alloy Al6061 rods, pre-compressed with different height reduction ratios (0, 10%, 30%, 50% and 70%), are prepared as the workpiece in the experiments. The experiment settings are given in Table 9.1. The signals of both cutting

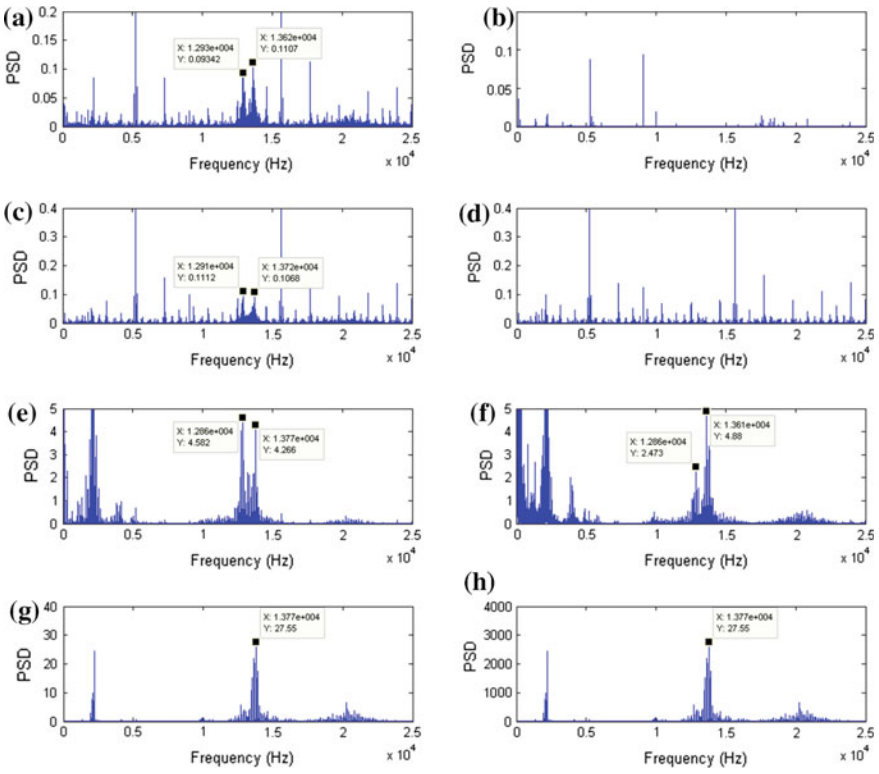

Fig. 9.2 Characteristic twin peaks in **a** coolant excitation only; **b** spindle stops, coolant OFF; **c** air-cutting with coolant; **d** air-cutting without coolant; **e** cutting of copper; **f** cutting of Al 6061; **g** cutting of brass and **h** cutting of bakelite

force and thrust force are recorded with a sample frequency of 50 kHz. Since different height reduction ratios influence the mechanical properties of the work materials, such features can be used to identify the changes of the characteristic peaks in the frequency domain.

For the purpose of comparison, two sets of experiments are designed. In Set A, the lubricant mist is turned on, while in set B, the lubricant mist is turned off. In both sets of experiments, the background signals are first obtained during air cutting. Then the signals of cutting force are taken for the cutting of aluminium alloy Al6061 rods with different height reduction ratios, 0, 10%, 30%, 50% and 70%. The machining parameters are kept constant in all experiments. In the present study, the investigation of the characteristic peaks is focused on cutting force signals only. The corresponding measurements of arithmetic roughness (R_a) and root-mean-square roughness (R_q) for each set of experiments are obtained by a surface profiler, Wyko NT8000.

The power spectrum density (PSD) plots based on the cutting force signals taken in sets A and B of the experiment are tabulated in the left and right columns of

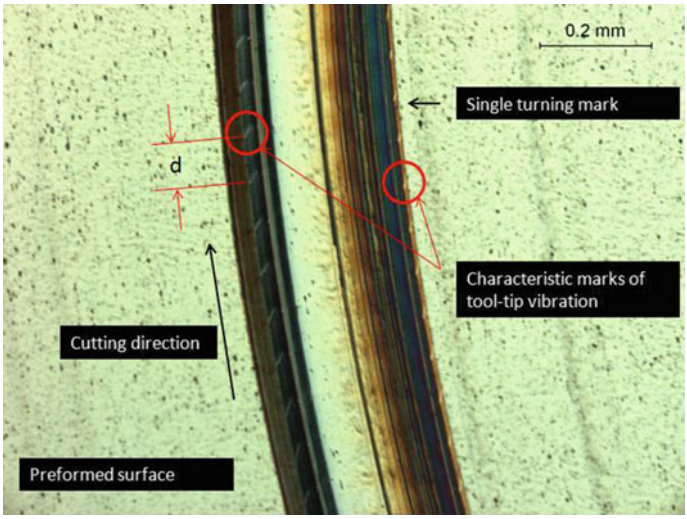

Fig. 9.3 Periodic *bar-shape* marks in the single turning mark on a preformed surface

Table 9.1 Experiment settings with different height reduction ratios (HRR) and cutting conditions

Sample no.	A	B
1	Air-cutting, lubricant ON	Air-cutting, lubricant OFF
2	0% HRR, lubricant ON	0% HRR, lubricant OFF
3	10% HRR, lubricant ON	10% HRR, lubricant OFF
4	30% HRR, lubricant ON	30% HRR, lubricant OFF
5	50% HRR, lubricant ON	50% HRR, lubricant OFF
6	70% HRR, lubricant ON	70% HRR, lubricant OFF

Fig. 9.4, respectively. The corresponding measurements of arithmetic roughness (R_a) and root-mean-square roughness (R_q) for each set of experiments are tabulated in Table 9.2.

As shown in Fig. 9.4a2, b2, the characteristic peaks are highlighted as P1 and P2, while such peaks are not found in other plots. In the frequency domain, P2 is located at about 14 kHz and another characteristic peak P1 is about 13 kHz lower than that of P2. Although many other peaks with smaller amplitudes are also observed in the PSD plots, they are ignored because there is no evidence that these peaks spring from the relative movement between tool tip and work material. As the peaks P1 and P2 are generated by the relative movement between cutting tool and work material, they are regarded as the dominant factors affecting surface roughness.

The frequencies of the characteristic peaks P1 and P2 for differently treated work materials are found to be not very sensitive to the cutting conditions, as shown in

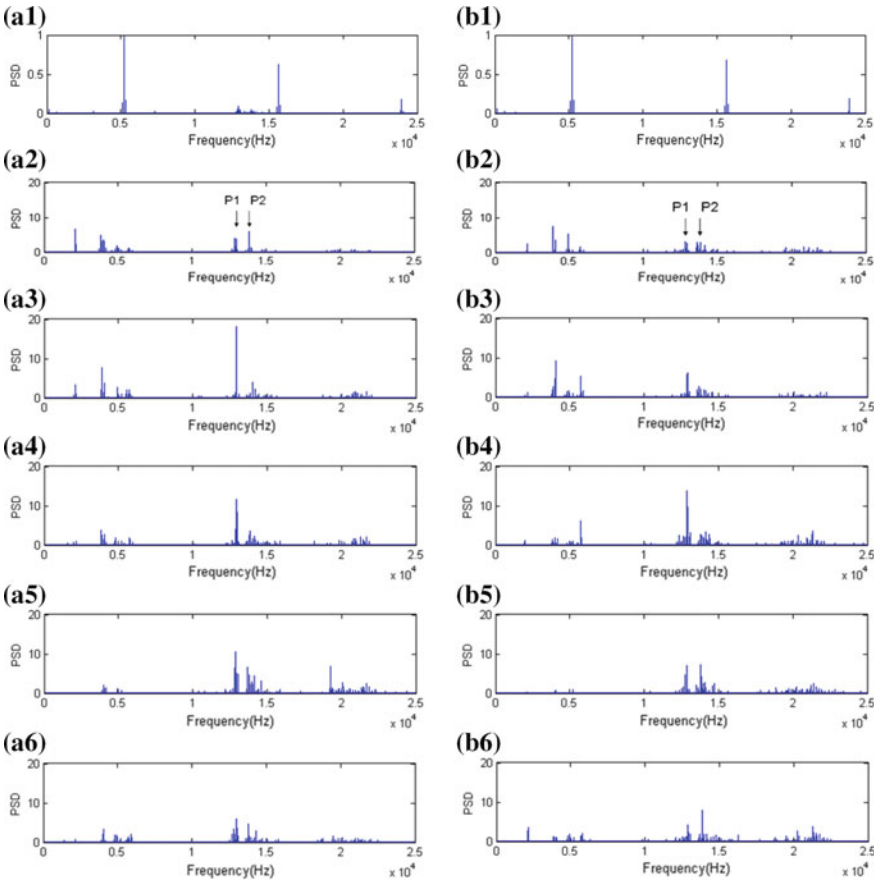

Fig. 9.4 Power spectrum density analyses of cutting force signals for experiment sets A (lubricant ON) and B (lubricant OFF), and (1) air cutting, (2) 0%, (3) 10%, (4) 30%, (5) 50% and (6) 70% height reduction ratio, respectively

Fig. 9.4. However, the amplitude of the peaks varies significantly. In order to describe the relative amplitude of the two peaks, an index named characteristic peak ratio (CPR) is defined in Eq. (9.2) below

$$\mathrm{CPR} = \frac{A_{P2}}{A_{P1}} \tag{9.2}$$

where A_{P1} and A_{P2} are the amplitudes of the two characteristic peaks P1 and P2. Based on the data in Fig. 9.4, the CPRs for both sets of experiments are drawn in Fig. 9.5. Therefore, the trend of the value of CPR with regard to the height reduction ratio can be identified. Furthermore, a correlation between the CPR index and surface roughness can be identified by comparing Figs. 9.5 and 9.6. For

Table 9.2 Surface roughness data (Wyko NT8000)

Reduction ratio (%)	Lubricant mist ON (Set A)		Lubricant mist OFF (Set B)	
	R_a (nm)	R_q (nm)	R_a (nm)	R_q (nm)
0	20.90	27.11	17.45	22.50
	20.74	26.14	21.00	27.02
	19.25	24.47	17.23	21.69
	30.24	37.65	18.97	21.28
	20.71	26.02	18.86	23.72
10	20.12	25.58	20.84	25.82
	18.46	23.28	21.86	27.39
	17.62	22.43	19.08	23.88
	19.49	24.30	19.58	25.29
	19.16	24.29	20.68	26.25
30	20.34	26.33	20.40	25.36
	20.04	25.63	17.92	22.47
	18.69	24.21	17.75	26.11
	19.75	25.08	17.21	21.72
	20.55	30.32	17.53	22.28
50	19.91	26.05	23.22	29.48
	19.02	24.26	19.82	25.43
	20.47	29.97	17.65	22.19
	22.45	29.91	23.39	29.38
	19.47	26.54	17.43	22.05
70	18.89	23.93	25.23	32.55
	19.45	24.32	20.51	25.67
	20.23	20.65	22.38	27.67
	19.48	24.34	25.92	32.98
	20.07	25.01	20.48	26.23

simplicity of analysis, only the arithmetic surface roughness (R_a) data are plotted in Fig. 9.6, since the values of root-mean-square roughness (R_q) show a similar trend to R_a. The minimum points of both the CPR index and R_a are found at 10 and 30% height reduction ratio in the experiment sets A and B, respectively. The trends described by the CPR index are in line with the surface roughness. Thus, the CPR index can be regarded as a reflection and predictor of surface roughness. Since the CPR index is directly derived from the signals of the cutting force in the micro-cutting process and surface roughness is the output of the surface measurement, the CPR index functions as a link between machining and measurement. On the other hand, the CPR index can be used to predict the quality of surface finish and to monitor the machining process, which also takes into account the mechanical properties of the work materials and machining conditions.

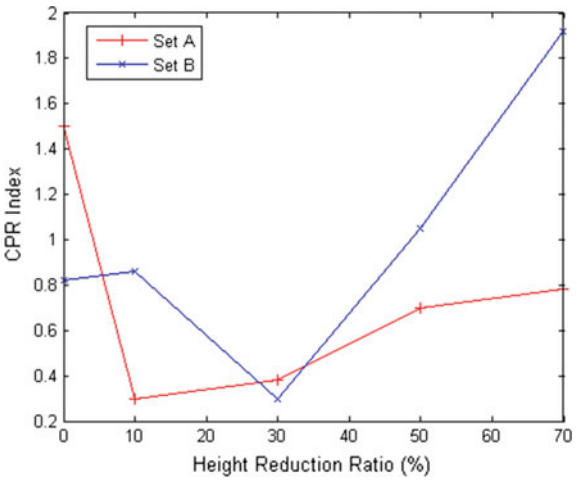

Fig. 9.5 CPR index in experiment Set A (with lubricant) and B (without lubricant)

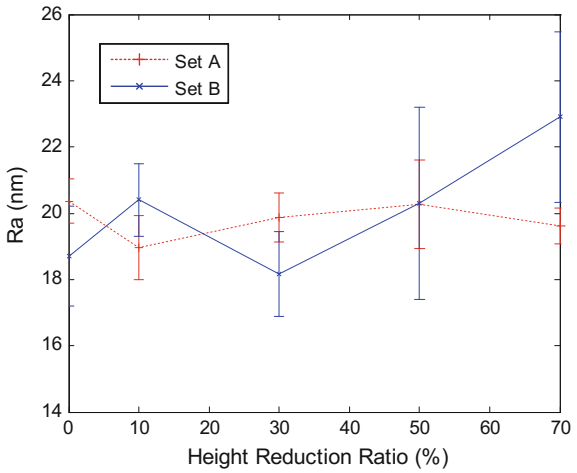

Fig. 9.6 Surface roughness (R_a) measured in experiment Set A (with lubricant) and B (without lubricant)

9.3 Modelling of Tool-Tip Vibration

9.3.1 An Impact Model Without Damping

A modified pendulum impact model is proposed to describe the tool-tip vibration during the cutting process. As shown in Fig. 9.7, the small amplitude assumption is adopted following Cheung and Lee (2000b), Takasu et al. (1985) and Bispink and Weck (1992), which implies that the angle θ is small enough to guarantee that the bob (or mass) of the pendulum impacts with the object wall A (with finite mass relative to the bob) deliberately placed perpendicularly (Fig. 9.7b). Thus, if the bob and the wall are regarded as two colliding particles, the direct impact between them

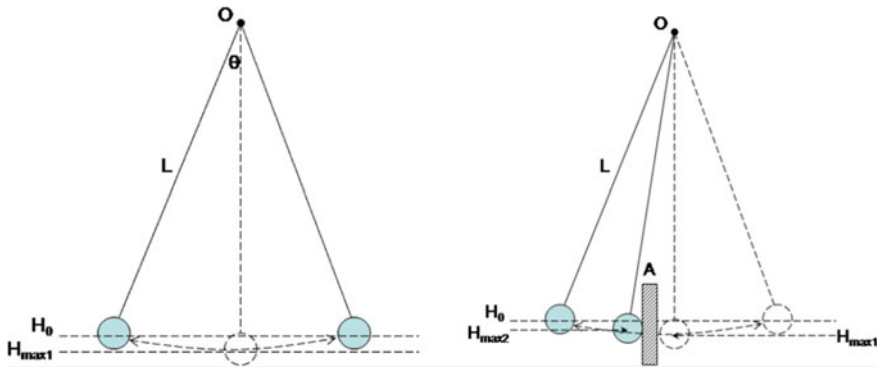

(a) Simple harmonic pendulum model (b) Pendulum impact model

Fig. 9.7 Simple physical model for tool-tip vibration

is collinear. By assuming that the momentum of the system is conserved during impact and that the impact is completely elastic, i.e. the coefficient of restitution equals 1. (although in Fig. 9.7 the bob and the wall are not represented by "points" geometrically, they are still regarded as particles rather than bodies in term of the physics), the trajectory of the bob can be described by the position function $h(t)$ of time t, as shown in Fig. 9.7, where H_0 is the initial position and $H_{\max}$ is the maximum distance from H_0 of the bob. It is assumed that the length of the pendulum measured from the pivot point to the bob's centre of gravity and the mass of the bob are constant.

Based on the assumption of small amplitude and no damping vibration, the model shown in Fig. 9.7a is a simple harmonic oscillator. The differential equation governing such motion is

$$\frac{\mathrm{d}^2\theta}{\mathrm{d}t^2} + \frac{g}{L}\theta = 0 \tag{9.3}$$

The solution to Eq. (9.3) can be expressed by a cosine function as

$$\theta(t) = \theta_0 \cos\left(\sqrt{\frac{g}{L}}t\right) \quad |\theta_0| \ll 1^\circ \tag{9.4}$$

where g is the local gravitational acceleration, L is the length of the pendulum measured from the pivot point to the bob's centre of gravity and t denotes the time. In such cases, the position function $h(t)$ of the bob can be expressed by a sinusoidal function in the form of Eq. (9.5):

$$h_1(t) = H_{\max 1} \sin(\omega_1 t + \phi_1) \tag{9.5}$$

$$\omega_1 = \frac{2}{T_0} = \frac{1}{\pi}\sqrt{\frac{g}{L}} \tag{9.6}$$

where ω_1 and ϕ_1 denote the frequency and phase of simple harmonic pendulum respectively; T_0 is the period of the pendulum. The trajectory of the bob can be expressed by the curve $h_1(t)$.

If an obstacle "wall" A is set to impact with the bob, and it is assumed that the mass of the wall is far larger than that of the bob, due to the momentum conservation in such system, the magnitude of the bob's velocity remains unchanged, but the direction is changed to the opposite when the impact happens. The pendulum impact model is shown in Fig. 9.7b. Based on the assumption of small amplitude, the trajectory of the bob can also be approximately expressed by a sinusoidal function as

$$h_2(t) = H_{\max 2} \sin(\omega_2 t + \phi_2) \tag{9.7}$$

where ω_2 and ϕ_2 denote the frequency and phase of the impact vibration model. According to the position of the wall A (Fig. 9.7b), the amplitude of the impact model is smaller than that of the free vibration model ($H_{\max 2} < H_{\max 1}$). The frequency of the impact model is higher ($\omega_2 > \omega_1$).

Therefore, due to excitation, the tool-tip vibration based on the proposed pendulum impact model can be formulated as the summation of Eq. (9.8) of the two vibrations expressed by Eqs. (9.5) and (9.7).

$$h(t) = h_1(t) + h_2(t) = H_{\max 1} \sin(\omega_1 t + \phi_1) + H_{\max 2} \sin(\omega_2 t + \phi_2) \tag{9.8}$$

According to the mathematics of fast Fourier Transform (FFT) and power spectrum density (PSD) analysis, the amplitude and phase of vibrations cannot be considered after the transformations. To investigate how FFT deals with the proposed impact model, a simplified form of Eq. (9.8) is expressed in Eq. (9.9) and the curves of function and the PSD plot of Eq. (9.9) are shown in Fig. 9.8 (for instance, ω_1 = 8.2 and ω_2 = 8.6, t = 0–10^4).

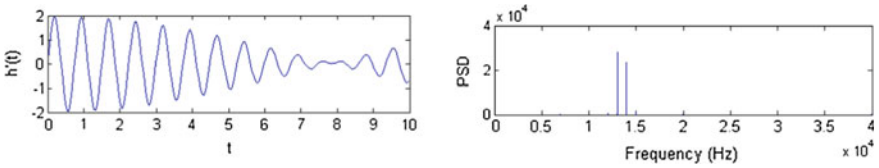

(a) h'(t) in time domain (b) twin peaks in PSD plot

Fig. 9.8 Twin peaks in PSD plot of the proposed impact model

$$h'(t) = \sin(\omega_1 t) + \sin(\omega_2 t) \tag{9.9}$$

Since the twin peaks identified in Figs. 9.8b and 9.4a2 are matched, the proposed model can be used to explain the emergence of the twin peaks. The impact model in Fig. 9.7b can be directly applied in the micro-cutting process, if the wall *A* in Fig. 9.7b is regarded as the tool-chip interface, the length of pendulum string as the tool shank length and the bob as the tool tip.

The proposed impact model of tool-tip vibration does not intend to account for all the possible factors leading to the formation of characteristic twin peaks in the PSD plots of Fig. 9.4. The proposed model is established based on the physical phenomenon (impact) in the micro-cutting process of SPDT, which is regarded as a dominant factor rather than an exclusive factor inducing the twin peaks. To substantiate the experimental results, the impact phenomenon is found to be present in all the non-ferrous materials tested in the present study. The tool tip is thus believed to vibrate in the course of machining along the cutting direction with twin frequencies. The high-frequency tool-tip vibrations are induced by the excitation of the applied forces (lubricant mist and impact with the work materials) while the characteristic twin peaks refer to the resonance frequency and the impact-induced frequency respectively.

9.3.2 *Non-harmonic Periodic Excitation with Process Damping Effect*

To further develop the model proposed in the preceding section, the conditions of excitation and the damping effect on the tool tip are investigated in this section. In a more realistic sense, the wall *A* in Fig. 9.7b is no longer assumed to be perfectly elastic to the bob of the pendulum in the emergence of impact. According to the idealised card model by Piispanen (1948) and the experimental observation and proposed model with load drop on the cutting force by Recht (1964), the cutting force can be neither constant nor regarded as a harmonic excitation to the tool tip in a dynamic system. Instead, from a macro-scale point of view on the elastoplastic behaviour of work materials, the cutting force can be qualitatively described as shown in Fig. 9.9. Though a constant cutting speed is employed in the cutting tests, the induced effective strain and strain rate on the material are never homogeneous, based on the elastoplastic behaviour of work materials, which in turn results in the non-harmonic periodic excitation to the tool tip.

According to the Fourier series of an arbitrary periodic function, the excitation force $f(t)$ can be expressed by the superposition of the harmonic equations as expressed in Eq. (9.10), where T is the period of cutting force and the calculations of corresponding coefficients are given in Eq. (9.11).

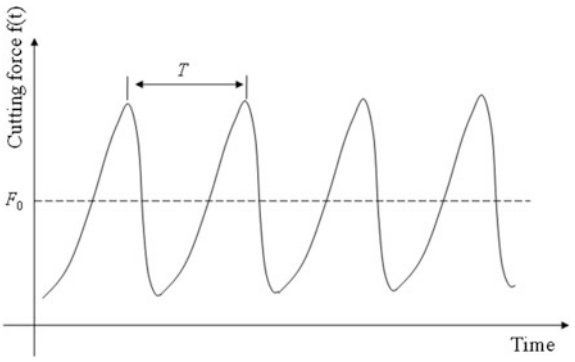

Fig. 9.9 Cutting force with a non-harmonic periodic nature as excitation to the tool tip

$$f(t) = \frac{a_0}{2} + \sum_{p=1}^{\infty} \left(a_p \cos p\omega_T t + b_p \sin p\omega_T t\right), \quad \omega_T = \frac{2\pi}{T} \tag{9.10}$$

$$a_p = \frac{2}{T} \int_{-T/2}^{T/2} f(t) \cos p\omega_T \mathrm{tdt}, \quad b_p = \frac{2}{T} \int_{-T/2}^{T/2} f(t) \sin p\omega_T \mathrm{tdt} \tag{9.11}$$

The damping factor in the tool-work or tool-chip dynamic system is a complex result of the damping factors within the work materials and the internal damping of the cutting tools. Moreover, the process damping is regarded as another damping factor, which is induced by the elastic recovery of the work materials to the clearance face of the cutting tool. The elastic recovery results in the "ploughing" or "rubbing" force which is also recognised in the literature. However, no previous work has pointed out the relationship between such process damping factor and tool-tip vibration, as well as surface roughness. In order to reveal the stress status in the micro-cutting process, a two-dimensional finite element (FE) model is proposed, following the methodologies described in the previous work by Wang et al. (2008) and utilising the commercial FE package MSC.Marc.

In the FE model, a simulation of orthogonal cutting is performed based on the assumption of plane strain. The diamond cutting tool is assumed to be rigid with a constant cutting speed and depth of cut. As in the actual cutting experiments, a small edge radius is employed in the geometric model. In order to focus on the elastic behaviour of the work material, and for simplicity, an isotropic constitutive model is adopted based on data on the mechanical properties of aluminium alloy Al6061. The displacement boundary conditions are utilised to restrict the plane movement of the nodes on the bottom of the work piece. Moreover, the advanced global remeshing option in MSC.Marc is activated to cope with the large distortion of the meshes in the geometric model. With this option, no predefined chip-work separation criteria are needed. The simulation result with chip generation is shown in Fig. 8.10. The diamond cutting tool is represented by a 2D curve, and the cutting

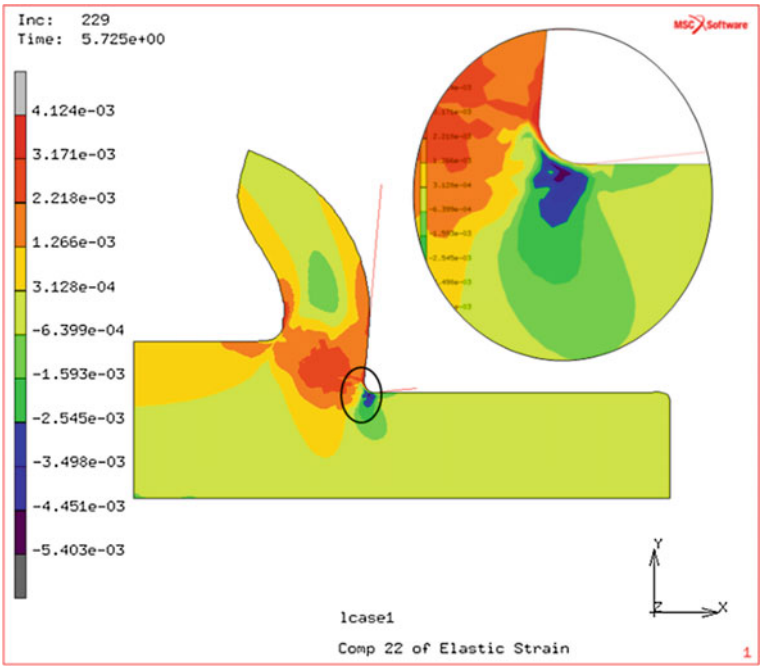

Fig. 9.10 Elastic strain in the thrust direction (Component 22, i.e. along the *Y*-axis in the model)

direction is along the negative *X*-axis. Component 22 of elastic strain (along the *Y* direction, i.e. the thrust force direction) is visualised and magnified in the inset. The dark blue region under the tool nose indicates that the elastic strain is imposed by the tool nose towards the negative *Y*-axis, which in turn exerts a reaction force to the tool nose, i.e. the thrust force. It is interesting to note that when the tool tip advances, i.e. on the removal of the imposed downward stress, the elastic stress stored in this area causes the material to spring back to accommodate the imposed elastic strain by the tool nose (Fig. 9.10).

The mechanism of process damping factor is shown in the schematic diagram in Fig. 9.11. Compared with the ideal case of the turned surface, the elastic recovery can be identified on the actual surface in the thrust direction with the tool advancing in the cutting direction. This effect of material recovery has also been reported by Kong et al. (2006). The circled area of chip root and the tool tip is magnified in the inset. The tool-tip moves between positions 1 and 2 due to vibration. When the tool moves from position 1 to position 2, the tool tip contacts the elastically recovered surface, which in turn yields the process damping factor. The process factor C_{proc} is added with the internal damping factor C_t as the total damping factor (C_{tt}) of the tool tip, as shown in Eq. (9.15). The dynamic system is modelled in Fig. 9.12, where *M, K* and *C* denote the mass, stiffness and damping, and the subscripts ct and tt denote the chip root and the tool tip, respectively. The term chip root is adopted to denote the contact area between the chip (work material) and the tool tip, which is

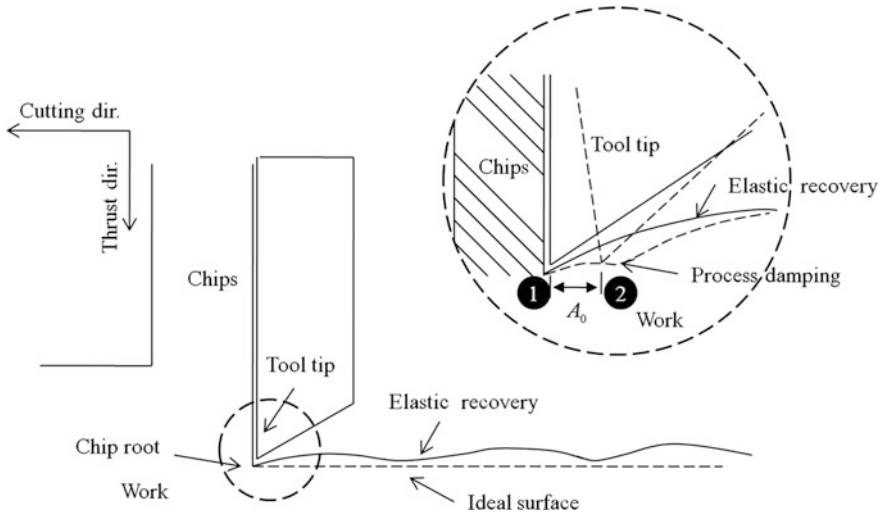

Fig. 9.11 Schematic diagram of elastic recovery and the generation of process damping factor on the clearance face of the diamond cutting tool

an effective area in the modelling of tool-tip vibration. Due to the nature of high frequency and small amplitude of the tool-tip vibration and the dynamic properties of ductile work materials, the effective area can be confined in a relatively small region, instead of the entire chip thickness, in the calculation. The dynamic system is expressed by Eq. (9.12), where ζ_{tt} and ζ_{cr} denote the damping ratio of the tool tip and chip root, as obtained in Eq. (9.14). The natural frequencies of the tool tip and the chip-root volume are denoted by ω_{tt} and ω_{cr}, respectively. The external excitation $f(t)$ can be expressed by Eq. (9.10).

$$\begin{bmatrix} \ddot{x}_{tt}(t) \\ \ddot{x}_{cr}(t) \end{bmatrix} + \begin{bmatrix} 2\zeta_{tt}\omega_{ntt} & 0 \\ 0 & 2\zeta_{cr}\omega_{ncr} \end{bmatrix} \begin{bmatrix} \dot{x}_{tt}(t) \\ \dot{x}_{cr}(t) \end{bmatrix} + \begin{bmatrix} \omega_{ntt}^2 & 0 \\ 0 & \omega_{ncr}^2 \end{bmatrix} \begin{bmatrix} x_{tt}(t) \\ x_{cr}(t) \end{bmatrix} = \begin{bmatrix} f(t)/M_{tt} \\ f(t)/M_{cr} \end{bmatrix} \tag{9.12}$$

$$\omega_{ntt} = \sqrt{K_{tt}/M_{tt}}, \quad \omega_{ncr} = \sqrt{K_{cr}/M_{cr}} \tag{9.13}$$

$$\zeta_{tt} = \frac{C_{tt}}{2\sqrt{K_{tt}M_{tt}}}, \quad \zeta_{cr} = \frac{C_{cr}}{2\sqrt{K_{cr}M_{cr}}} \tag{9.14}$$

$$C_{tt} = C_t + C_{proc} \tag{9.15}$$

The natural frequency of the tool tip ω_{tt} represents the frequency of the right peak of the characteristic twin peaks. Due to the process damping factor C_{proc}, the resultant frequency will shift to the left, such that the left peak of the characteristic twin peaks is presented. The process damping also reduces the amplitude of the tool-tip vibration, due to its nature in energy dissipation. Therefore, the proposed

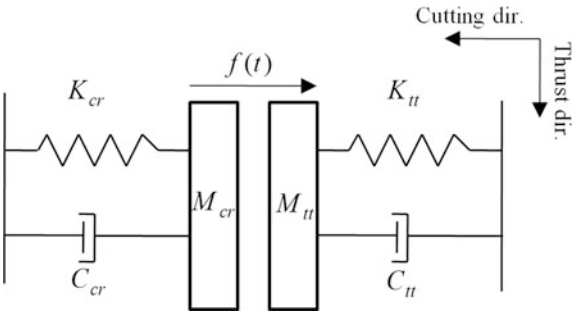

Fig. 9.12 A dynamic model of the system of tool tip and the effective volume of work material

CPR index in Eq. (9.2) is also an index of the process damping factor. In the following sections, it can be seen that the process damping factor is a key factor affecting the surface roughness.

Differing from the previous dynamic models of cutting systems in the literature, the presented model studies the tool tip and the small volume of chip-root material at the microscopic scale. This model does not intend to add more factors or to study the dynamic behaviour of the cutter and the whole workpiece. Instead, the proposed model extracts the chief characteristics of interest from the complex system, and is utilised to explain and correlate with the experimental results. Furthermore, the proposed model with the process damping factor can also be utilised to establish a relationship between the tool-tip vibration and surface roughness.

The process damping factor can also be added into the previously proposed impact model of the pendulum system (Fig. 9.13). Due to the elastic recovery of the turned surface beneath the clearance face of the cutting tool, a friction force (*f*) is generated by the relative displacement of the tool tip and the recovered surface.

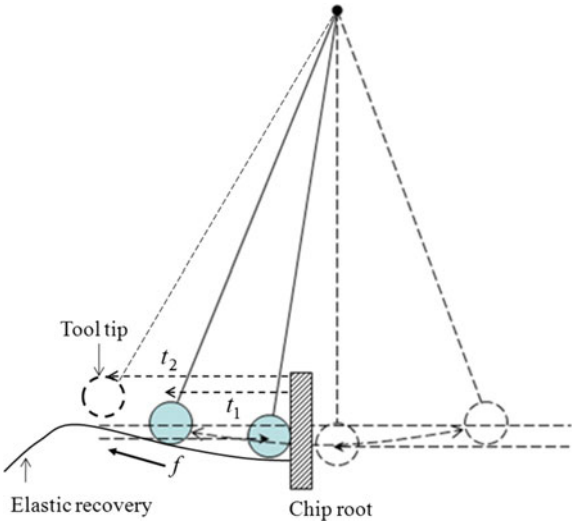

Fig. 9.13 Revised pendulum impact model with the effect of process damping

Such friction force can reduce the kinetic energy of the bob of the pendulum, i.e. the tool tip in vibration. Therefore, the period half time increases from t_1 to t_2, and the frequency decreases to form the left peak of the characteristic twin peaks. In this theoretical model, the chip root is actually an excitation to the tool tip that forms the right peak. In such manner, the characteristic twin peaks are generated.

9.4 Representative Measurement Method

9.4.1 Influence of Tool-Tip Vibration on the Machined Surface

In the literature, the low-frequency process vibration has been extensively studied with its effect on surface roughness. However, high-frequency tool-tip vibration in the cutting force direction, is an intrinsic feature of ultraprecision single-point diamond turning (SPDT). The effect of the high-frequency vibration on surface generation was also supported by Hocheng and Hsieh (2004). Research work covers several key aspects of the problem, including (1) the modelling method for dynamic machining system and chatter mechanisms, (2) the relationship between vibration and surface roughness, (3) vibration direction and frequency range, (4) the effect of material swelling and recovery on tool vibration and process damping, (5) surface characterisation methods, (6) process vibration and material factors, etc.

This section is dedicated to studying of the influence of tool-tip vibration on surface roughness. The resulting periodic fluctuation of the surface profile is identified in a particular spatial frequency range by a tangential measurement method. The ISO standard provides merely a minimal, not an optimal requirement for surface measurement. To this end, a representative measurement method is proposed to better characterise the machined surface in SPDT. The conventional radial and aerial surface measurements yield a relatively biased result on surface roughness which cannot adequately reflect the detrimental effect of tool-tip vibration. Representative measurement takes account of the sample area ratios and is able to be used to objectively study the discrepancies in surface measurement. The proposed model for surface generation and representative measurement are applicable to problems in the surface generation in ultraprecision SPDT, such as the spiral turning marks and spatial errors in radial profile measurement.

This section tackles the problem of representative measurement of nano-surfaces machined in single-point diamond turning. With stylus-type measurement equipment, such as a Form Talysurf system, 2D profile measurement was conducted (Cheung and Lee 2001; Abouelatta and Mádl 2001). A special kind of measurement is radial measurement (To et al. 2001; Hocheng and Heieh 2004; Cheung and Lee 2000a), in which the data of the measured profile can be readily transformed into the spatial frequency domain with FFT. With the interferometer surface profiler, the aerial data or 3D measurement of surface roughness can be recorded (Li et al. 2010;

Lee and Cheung 2001; Hocheng and Heieh 2004). As an advantage, the aerial data contain the surface information for both cutting direction and radial direction, with which the effect of tool-tip vibration along the cutting force direction can be studied. In this chapter, a special data processing method is employed to extract the profile data along turning marks, in which the resultant profile of relative tool-work vibration can be clearly observed. Furthermore, a representative measurement method is proposed to characterise the surface roughness, based on the introduced sample area ratios (η). A η-sensitive surface roughness $\left(\widetilde{R}\right)$ is introduced to investigate the effect of sample area ratios and tool-tip vibration. The representative measurement is thereby conducted in the low-η, high-η and oversampling regions. The proposed representative measurement complies with, but is not restricted to, the international standard (ISO 4288:1996).

9.4.1.1 Cutting Experiments

Two face turning experiments were conducted to examine the influence of tool-tip vibration on surface roughness (Table 9.3). In Experiment 1, a polycrystalline OFHC copper specimen was machined with a depth of cut of 10 μm and a feed rate of 20 mm min^{-1} with a spindle speed of 2000 rpm. The average grain size of the OFHC copper specimen was 75 μm. The specimen was in the shape of a cylinder with a diameter of 12.7 mm. The tool nose radius was 2.503 mm. A coolant mist was used and sprayed towards the tool-chip interface through a nozzle. The copper specimens were flattened first with the same machining parameters to remove the possible tilt angle of the sample surface incurred in the mounting procedure. Then the material was removed to a depth of 50 μm by face turning with five passes to ensure the constant onward depth of cut of 10 μm in the experiments.

In Experiment 2, a cylindrical specimen of copper single crystal was prepared with a diameter of 12.8 mm. The initial crystallographic orientation of the normal of machining surface was determined by an X-ray diffractometer. In this chapter, the (111) surface was selected to be machined on a two-axis single-point diamond turning machine (Optoform 30, Taylor Hobson Co.). The face turning was performed at a depth of cut of 10 μm, and a feed rate of 20 mm min^{-1} with a spindle speed of 8000 rpm. The tool nose radius was 0.5329 mm. A Kistler 9252A force transducer was mounted with a pre-loading force between the tool shank and the tool post. A 14-bit multifunction Data Acquisition (DAQ) card (PCI-6132, National Instrument) was installed on a PC workstation to convert the analogue signals of the

Table 9.3 Machining parameters for the face turning experiments

Exp. no.	Depth of cut (μm)	Feed rate (mm min^{-1})	Spindle speed (rpm)	Specimen
1	10	20	2000	Polycrystalline copper
2	10	20	8000	Cu (111)

cutting forces. Using the Kistler 5011B charge amplifier, the converted signals were recorded at the sampling rate of 1 MHz using the LABVIEW software package. The signals of the cutting force were further processed using fast Fourier transform (FFT) and studied in the frequency domain.

The geometric features of the machined surface were further characterised by an interferometric surface profiler Wyko NT8000 and an optical microscope Olympus BX60. To examine surface roughness, five sample areas were selected along the radial direction on the machine surface and were numbered from 1 (close to the centre of the machined surface) to 5 (away from the centre of the machined surface), at distances of 0.7, 0.9, 1.4, 1.7 and 2 mm from the centre, respectively. In accordance with (ISO 4288:1996), in each sample area, the surface profile data were taken five times, with sampling lengths not shorter than 0.08 mm. *R*-parameters were employed to characterise surface roughness, including arithmetic average roughness (R_a), root-mean-squared roughness (R_q), maximum height of the profile (R_z) and the average distance between the highest peak and lowest valley (R_t), as shown in Eq. (6.1), where y_i are the profile data, $R_{v(p)} = \min(\max) y_i$, s is the number of sampling and R_{ti} is the R_t for the ith sampling length (ASME 1996).

$$R_a = \frac{1}{n}\sum_{i=1}^{n} |y_i|, \tag{9.16a}$$

$$R_q = \sqrt{\frac{1}{n}\sum_{i=1}^{n} y_i^2}, \tag{9.16b}$$

$$R_z = \frac{1}{s}\sum_{i=1}^{s} R_{ti}, \tag{9.16c}$$

$$R_t = R_p - R_v. \tag{9.16d}$$

In the measurement of surface roughness, considering the influences of tool-tip vibration on surface generation, different sampling lengths resulted in different *R* values. Besides the suggested sampling lengths by the ISO standard, sampling lengths of 0.04 and 0.12 mm were also adopted to calculate the *R* values. Furthermore, different sample area ratios (the sample area over the machined area) also led to discrepancies in the calculated *R* values. This phenomenon was studied with the sample area ratio increasing from 10 to 200%, i.e. "oversampling" on the machined surface.

In each sample area, the aerial data of the surface profile were recorded by an interferometer, Wyko NT8000. Taking into consideration the process of surface generation and the critical factor of tool-tip vibration, the aerial data were decomposed into two linear compositions, along the radial and along the tangential directions of a selected turning mark, respectively. Such decomposition of aerial

data can also be regarded as the measurement of the surface profile in a stylus mode, along a predefined sampling path. The importance of such decomposition and the effect of tool-tip vibration along the tangential direction are described in the following sections. The relationship between tool-tip vibration and surface generation can only be identified from the tangential data. On the other hand, the radial data possess a random nature and a diminished value due to the overlap of scallops resulting from adjacent turning marks. Compared with the tangential data, the radial data are not as significant in relation to explaining the generation of surface roughness, thus, they are excluded from the investigation in this chapter.

9.4.1.2 Identification of Tool-Tip Vibration on the Machined Surface Profile

The digitised signals of cutting force and thrust force are converted and studied in the frequency domain using fast Fourier transform. The power spectrum density (PSD) is further employed to characterise the signals. According to previous study of the characteristic twin peaks found in the PSD plots (Wang et al. 2010), similar twin peaks are also identified in Experiments 1 and 2. In this chapter, for both single crystal Cu(111) specimen (Fig. 9.14b) and polycrystalline copper specimen (Fig. 9.14c) with different spindle speeds, the twin peaks can always be observed in the high-frequency interval of cutting forces, ranging from 12 to 14 kHz. On the other hand, no peaks with significant power spectrum density can be located in such a high-frequency range for thrust forces. On the contrary, the thrust force signals are intrinsically located in the frequency range lower than 100 Hz, as studied by Lee and Cheung (2001). However, this low-frequency thrust force does not directly contribute to the relative tool-work displacement; thus, only the cutting force should

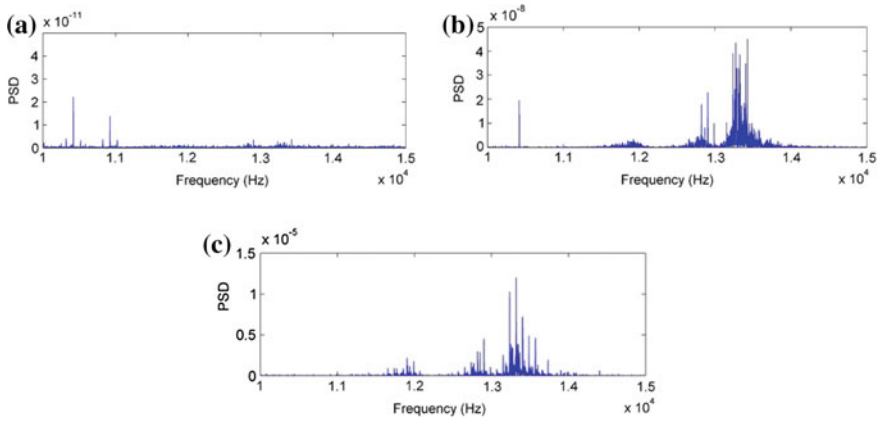

Fig. 9.14 Power spectrum density plot of measured force signals: **a** thrust force in Experiment 2; **b** cutting force in Experiment 2 and **c** cutting force in Experiment 1

be included in the study of the mechanism of surface generation, and the modelling of the micro-cutting process.

An intrinsic property of the tool-tip vibration at 14 kHz, is utilised to reveal its influence on the profile of machined surface. In Experiment 2, the tangential data of the surface profile in a single turning mark are measured at a distance of 1.25 mm from the centre of the workpiece. The peak-to-peak distance $\left(d_{\mathrm{pp}}\right)$ due to tool-tip vibration can be expressed as Eq. (9.17), where D is the distance from the turning mark to the centre of the workpiece, S is the spindle speed and f_{ttv} is the frequency of the tool-tip vibration, which is approximately assigned 14 kHz in the calculation.

$$d_{\mathrm{pp}} = \frac{2\pi \cdot \mathrm{SD}}{60 f_{\mathrm{ttv}}} \tag{9.17}$$

In Fig. 9.15, the measured distance is about 75 μm on average. On the other hand, the calculation can be conducted at $D = 1.25$ mm and $S = 8000$ rpm, which results in a peak-to-peak distance of 0.0748 mm and a spatial frequency of 13.33 mm^{-1}. This result indicates that the influence of tool-tip vibration is significant on surface generation. The tool-tip vibration in the direction of the cutting force also induces the relative tool-work displacement in the direction of thrust force, and in turn, results in the periodic fluctuation of the surface profile during the micro-cutting process.

Since tool-tip vibration takes place at a fixed frequency during the turning of the entire surface of the specimen at a constant spindle speed, the linear velocity, or surface speed, is proportional to the distance from the location of the cutting tool to the centre of the workpiece.

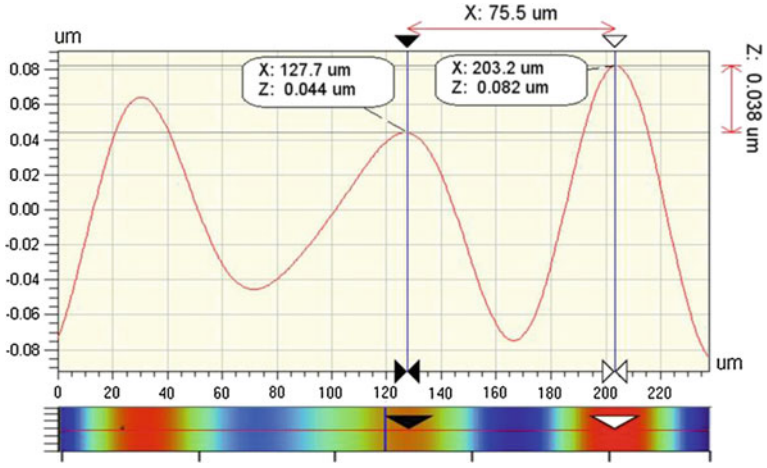

Fig. 9.15 The surface profile in a single turning mark at a distance of 1.25 mm from the centre of the workpiece

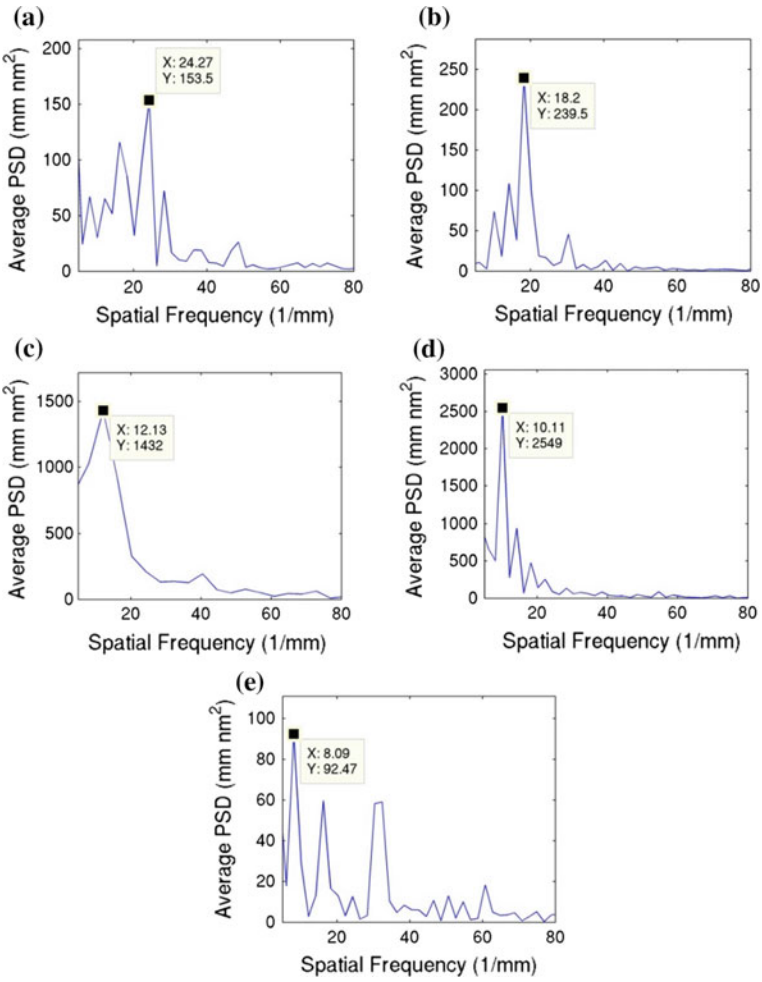

Fig. 9.16 Left shift of identified peak at sample location 1–5 (**a**–**e**) in Experiment 1, *X* spatial frequency, *Y* average PSD

As designed in the experiments, the surface power spectrum density plots are calculated at the five sample areas along the radial direction, from 1 (close to centre of the workpiece) to 5 (away from centre of the workpiece). In each sample area, the spatial frequency is calculated along the tangential data of the surface profile, which contains the characteristics of tool-tip vibration, as proven above. In Fig. 9.16a–e, the peaks corresponding to the frequency of tool-tip vibration are indexed. A left shift to low spatial frequency can be observed, which results from an increase in surface speed.

This new method of measurement and calculation builds up a link between the temporal and the spatial frequencies in the micro-cutting process. The relationship

Table 9.4 Spatial frequency and converted temporal frequency

Sample location	1	2	3	4	5
Spatial freq. (1/mm)	24.27	18.2	12.13	10.11	8.09
Converted temporal freq. (Hz)	14,225	13,715	14,219	14,391	13,548

between spatial frequency and temporal frequency can be expressed as $f_{\text{spatial}} = (60 / 2\pi\,\text{SD}) f_{\text{temporal}}$. The radial distance of the five sample areas are 0.7, 0.9, 1.4, 1.7 and 2 mm from the centre, respectively. Based on the measured spatial frequency, the converted temporal frequency is shown in Table 9.4 as below. A good estimation of the frequency of HFTTV can be found around 14 kHz.

In Experiment 2, further observation of the machined surface reveals the "spiral" shaped marks intersecting with the turning marks, as shown in the micrograph of Fig. 9.17a. The square area defined by broken yellow lines is magnified in Fig. 9.17b. The tangential profile of a length of 0.1 mm is selected along a single turning mark in the cutting direction. The spatial frequency is about 90 mm^{-1} calculated in Fig. 9.17b, which is about 0.2 mm from the centre of the workpiece. Substituting all the parameters into Eq. (9.17), $d_{\text{pp}} = 2\pi \times 0.2 \times 8000/(60 \times 14{,}000) = 0.012$ mm. Thus, the calculated spatial frequency is 1/0.012 = 83.33 mm^{-1}, which is of the same order as the measured spatial frequency.

Tool-tip vibration directly leads to relative tool-work displacement in surface generation. The relative distance between the tool-tip and the machining surface determines the process of material removal and other machining-related factors, such as cutting force, depth of cut and material removal rate, etc. The high-frequency tool-tip vibration in the direction of the cutting force is of paramount importance in understanding the micro-cutting process and surface generation. However, direct evidence is still missing to verify the relationship between low-frequency vibration in the direction of the thrust force and surface generation.

9.4.2 *Effect of Sample Locations on Surface Roughness*

As mentioned above, the tool-tip vibration factor is taken into consideration throughout the analysis. On the machined surface, the surface roughness values at the sample locations 1–5 are calculated using the aerial profile data, and are plotted in Fig. 9.18. With the same sampling length of 0.08 mm and sampling area of 0.08 mm by 0.08 mm at all the sample locations, the R values for peak-to-valley differences, R_t and R_z, increase significantly with increasing distance from the sample location to the centre of the workpiece. However, the arithmetic average R value (R_a) does not follow the same trend. Due to the existence of tool-tip vibration, the inner sample locations contain as many more complete cycles of fluctuations than do the outer sample locations for the fixed sample area, due to the dependency on the radial distance (D) as expressed by Eq. (9.17). On the other

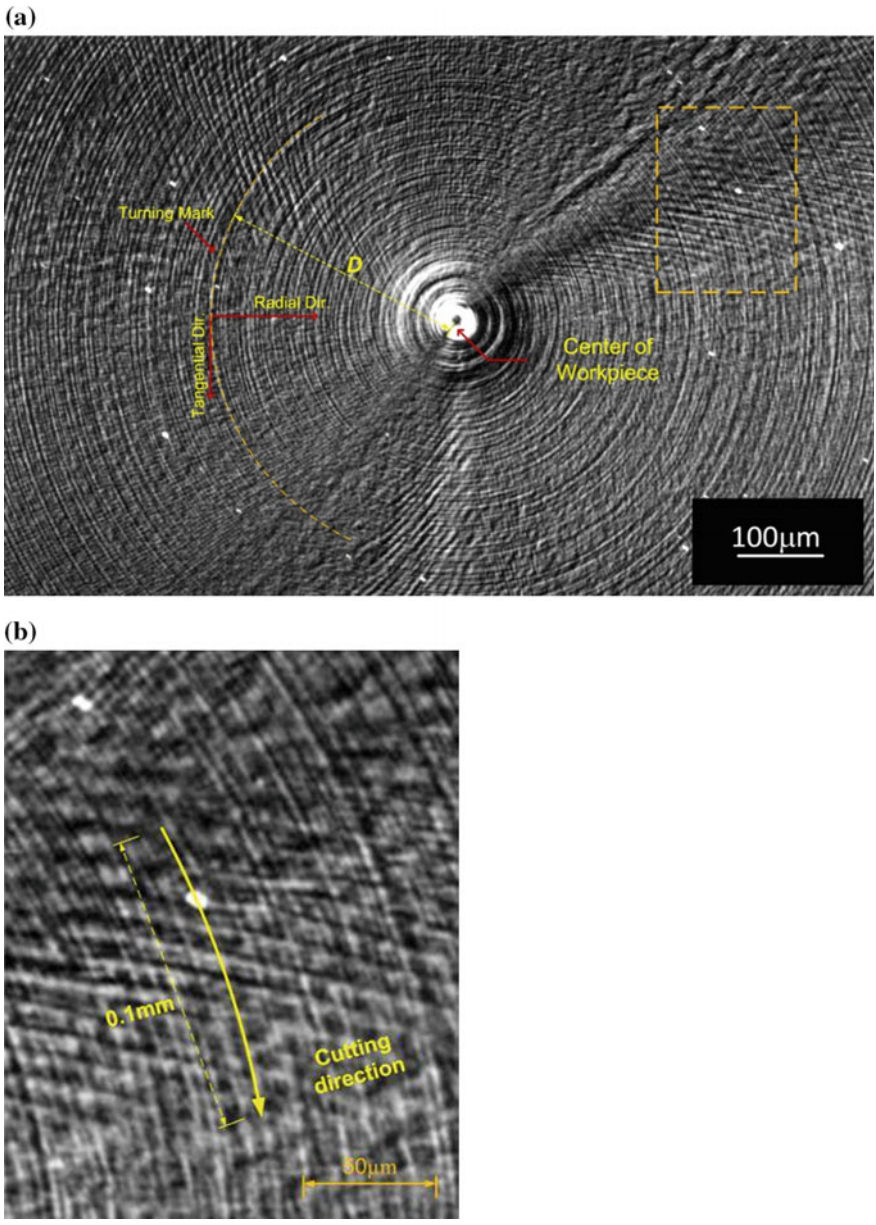

Fig. 9.17 Micrograph of **a** the machined surface in Experiment 2 and **b** the magnified part of spiral marks at D = 0.2–0.3 mm

hand, any machined surface must have a certain degree of surface waviness due to the precision of the machine tool, and single-point diamond turning possesses high form accuracy in the sub-micrometre range. Thus, from a statistical point of view,

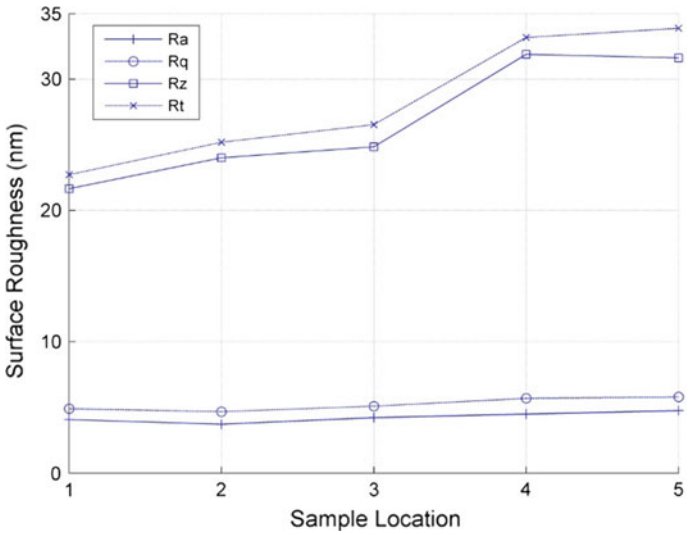

Fig. 9.18 Measured R values of machined surface at sample locations 1–5 of Experiment 1

the inner sample location, which contains more cycles of surface fluctuation, is less sensitive to the effect of surface waviness, and in turn, a smaller peak-to-valley R value is ensured. On the other hand, a much larger value is likely to occur in the outer sample locations. However, the effect of surface waviness is never uniform, due to the nonlinear nature of the waviness itself at different sample locations. Therefore, the increase of the peak-to-valley R values is not linear either. In this regard, the experimental observation is compatible with our proposed model. Furthermore, it is well recognised that higher cutting (surface) speed is prone to generate a surface with greater surface roughness, as can be seen from the simulated and measured surface roughness in the work by Jang et al. (1996), and the cutting trials on single-point diamond turning in the work of Li et al. (2010). This is also in line with the measured surface roughness in this chapter, where both the surface speed and surface roughness increase, as the sample location becomes farther away from the centre of the workpiece.

9.4.3 *Effect of Sample Area Ratios and Representative Measurement*

Besides the sample locations, the effect of sample area ratios on surface roughness is studied in this section. The concept of a sample area ratio (η) is first specially introduced to characterise the sampling effects on surface roughness in ultraprecision machining, with respect to the physical phenomenon of tool-tip vibration. The

sample area ratio is defined as the tool sample area over the total area of the machined surface, where oversampling is allowed on the machined surface. With the sample area ratio, the corresponding R values are redefined as η-sensitive R values $\widetilde{R}_{(x)}$. In such manner, the calculation of $\widetilde{R}_{(x)}$ follows the rule given in Eq. (9.18a), where the R values obtained at jth sample location are denoted by $R^j_{(x)}$, A^j is the corresponding sample area, A_{total} is the total area of the machined surface and the Einstein summation applies. An example of the derivation of $\widetilde{R}_z$ is given in Eq. (9.18b), where s is the sampling number.

$$\eta = \frac{\sum A^j}{A_{\text{total}}} \times 100\%, \quad \widetilde{R}_{(x)} = \frac{A^j R^j_{(x)}}{A_{\text{total}}} \tag{9.18a}$$

$$\widetilde{R}_z = \frac{A^j R^j_z}{A_{\text{total}}} = \frac{A^j \left(\frac{1}{s}\sum_{i=1}^{s} R^j_{ti}\right)}{A_{\text{total}}} \tag{9.18b}$$

Differing from the traditional definition of R value, whose raw data originated from a single area or a small number of sample areas, i.e. with a low η value, the η-sensitive $\widetilde{R}$ values characterise the entire machined surface in an unbiased manner. The two variables A and j in the definition of $\widetilde{R}$ (Eq. 9.18a) can be adjusted to comprehensively study surface roughness with respect to different sample areas and different numbers of samples, i.e. the η value. Using the concept of sample area ratio, the study of surface roughness can be divided into three regions: the low-η, high-η and oversampling regions.

Due to the effect of tool-tip vibration, the machined surface can be categorised as "periodic" because it has a particular surface texture or pattern. A periodic surface like that in Fig. 9.17a, is representative of the characteristics of the machined surface, if all the sample areas are selected along the radial direction with an increasing distance from the centre of the workpiece. In the machined surface of Experiment 2, a series of sample areas of 40 μm by 40 μm, 80 μm by 80 μm and 120 μm by 120 μm are employed to plot the η-sensitive $\widetilde{R}$ values, with different numbers of sample areas. The normalised η-sensitive surface roughness values are plotted against sample area ratios in Fig. 9.19. Based on Fig. 8.18, R_a and R_q, R_z and R_t follow the same trend respectively; thus, for the sake of simplicity only $\widetilde{R}_a$ and $\widetilde{R}_t$ are selected to appear in Fig. 9.19 where $\widetilde{R}'_{(x)}$, $\widetilde{R}_{(x)}$ and $\widetilde{R}''_{(x)}$ stand for the measured roughness with the sample areas of 40 μm by 40 μm, 80 μm by 80 μm and 120 μm by 120 μm, respectively. Normalised values are utilised to ensure that all the curves can be presented to the same scale.

The low-η region is defined below as having a sample area ratio less than 50%, in which region all the η-sensitive $\widetilde{R}$ values change dramatically, with a large standard deviation. The high-η region is located between 50 and 100%, in which region the variation of the $\widetilde{R}$ values tends to be smooth. Over 100% of the sample

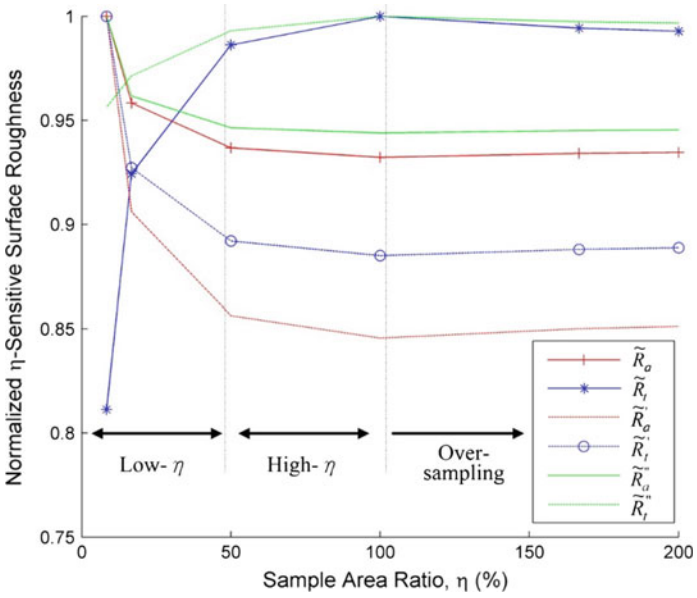

Fig. 9.19 Normalised η-sensitive R values in Experiment 1

area ratio is the oversampling region, in which more sampling does not yield a significant modification of the $\widetilde{R}$ values. In the low-η region and for the sample area of 80 μm by 80 μm, if the effect of surface waviness is neglected, small surface coverage leads to lower peak-to-valley values $\left(\widetilde{R}_t\right)$ far from the centre of the workpiece but shows a higher arithmetic average roughness $\left(\widetilde{R}_a\right)$ at the same time. Such biased sampling results are improved in the high-η region, where all the η-sensitive $\widetilde{R}$ values become stable with smaller standard deviations. As for the oversampling region, no further improvement can be found, since the machined surface is fully characterised in the high-η region.

If an ideal case is assumed without the uncertainty induced by surface waviness, a schematic diagram of the sampling area and the η-sensitive $\widetilde{R}$ values would appear as shown in Fig. 9.20. At different distances from the centre of the workpieces D1 and D2, the same sampling area yields different results for a sampled profile. When D1 $\ll$ D2, the sampled profile contains at least several complete cycles of fluctuation at D1, while only a part of a cycle is windowed at D2. In Fig. 9.20, the η-sensitive $\widetilde{R}$ values are calculated in the low-η region, which in turn results in a small peak-to-valley R value. If the sample area ratio is increased, no matter if it is by increasing (1) the unit sample area or (2) the number of sample areas, more complete cycles of surface profile fluctuation can be included in the calculation; therefore, a large peak-to-valley R value can be obtained.

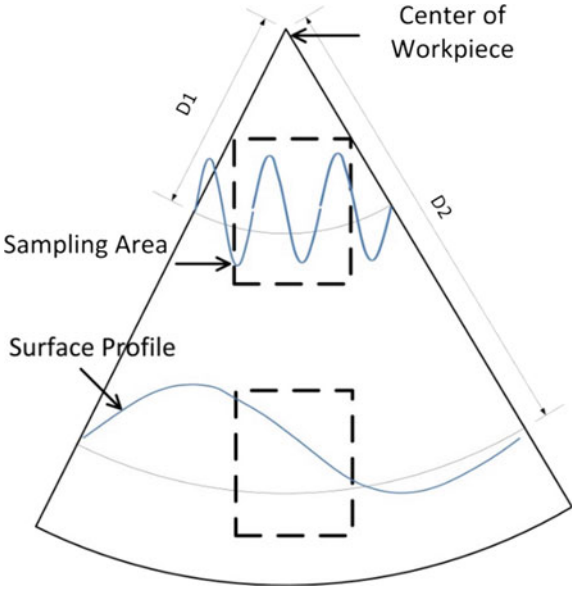

Fig. 9.20 A schematic of the sampling area and the effect on the calculation of the η-sensitive values

A suggested sampling length of 80 μm is given in the ISO standard (ISO 4288:1996) for roughness in the range smaller than 20 nm; however, this value does not take into consideration the important factor of tool-tip vibration in surface generation of single point diamond turning. Based on our theory, a sampling length of 80 μm is applicable with the maximum distance from the centre of the workpiece $D_{\max}$ given by Eq. (9.19), which is derived from Eq. (9.17) for the case when a single sample area is employed.

$$D_{\max} \leq \frac{0.08 \times 60 f_{\text{ttv}}}{2\pi \cdot \text{S}} \tag{9.19}$$

In the low-η region of Fig. 9.19, with the smallest sample area, both $\widetilde{R}'_a$ and $\widetilde{R}'_t$ decrease when the sample area ratio increases. When larger sample areas are employed, the trend of $\widetilde{R}_a$ and $\widetilde{R}''_a$ remains the same as $\widetilde{R}'_a$, but the trend of $\widetilde{R}_t$ and $\widetilde{R}''_t$ becomes the opposite of $\widetilde{R}'_t$. This observation indicates that a sampling length far shorter than $2\pi \cdot \text{SD}/60 f_{\text{ttv}}$ is prone to yield a biased characterisation of the surface. According to Eq. (9.19), a larger sample area is required when the sample location is farther from the centre of the workpiece. However, when the sample area is larger than adequate, as with the 120 μm by 120 μm in Fig. 9.19, no further improvement in surface roughness can be identified. From the aspect of the sample area ratio, this sample area also results in an oversampling region.

According to the above analysis, it can be concluded that better sampling can be achieved by a larger unit sample area or an increased number of sample areas. With the introduction of the concept of η-sensitive $\widetilde{R}$, a generic guideline for sampling is

to avoid the low-η region when measuring surface roughness within sample areas. In other words, a representative measurement should be made in the high-η region, from which the result obtained can be used to characterise the surface finish.

9.5 Modelling and Characterisation of Surface Roughness Generation

9.5.1 Surface Generation Model with Tool-Tip Vibration

High-frequency tool-tip vibration in the cutting force direction is simplified and modelled by a sinusoidal wave during the face turning process. In an ideal case where the extreme precision of the machine tool leads to negligible surface waviness, the turning process can be regarded as a surface roughening process with the cutting tool moving along the sinusoidal wave at a constant spindle speed. According to the experimental observations and previous analysis, the vibration takes place in the full frequency spectrum of the dynamic system, including low- and high-frequency vibration. However, only the effect of high-frequency tool-tip vibration is significant enough to induce relative tool-work displacement, which in turn roughens the surface. Therefore, a typical sinusoidal wave is employed in the modelling, as expressed by Eq. (9.20).

$$z = z_0(t) + z_{\text{ttv}}(t) = z_0(t) + A_{\text{ttv}} \sin(2\pi\omega t + \varphi_0) \tag{9.20}$$

The general model is defined by Eq. (9.20), where the location of the cutting tool is the function of cutting time t, and the profile of the machined surface consists of two components: the waviness $z_0(t)$ and roughness induced by the tool-tip vibration $z_{\text{ttv}}(t)$. In reality, all kinds of factors, including the precision of the machine tool, dynamic performance and material-related factors, determine that the two components are time-dependent variables. If both components are studied from the aspect of periodic functions, the frequency of $z_0(t)$ is lower than that of $z_{\text{ttv}}(t)$ by several orders of magnitude. In this section, the first component is assumed to be time-independent, i.e. the waviness is small enough to be ignored. Since the aim of the proposed model is to explain the effect of tool-tip vibration on surface generation instead of obtaining the exact values, the amplitude of tool-tip vibration A_{ttv} and the frequency ω are assumed to be constant. This also agrees with the experimental results (Wang et al. 2010) in that no obvious shift in the frequency of the characteristic twin peaks was observed.

Based on the model proposed in Eq. (9.20), the 3D surface is plotted (with $\omega = 14$ kHz and $A_{\text{ttv}} = 150$ nm) in Fig. 9.21a, with its contour plot, by projection of the profile data on the sample area. In Fig. 9.21a, the peaks and valleys are coloured orange and blue, respectively. The small black dots denote the extreme values on the surface profile. The pattern of the simulated surface profile is further verified by the experimental result shown in Fig. 9.21b.

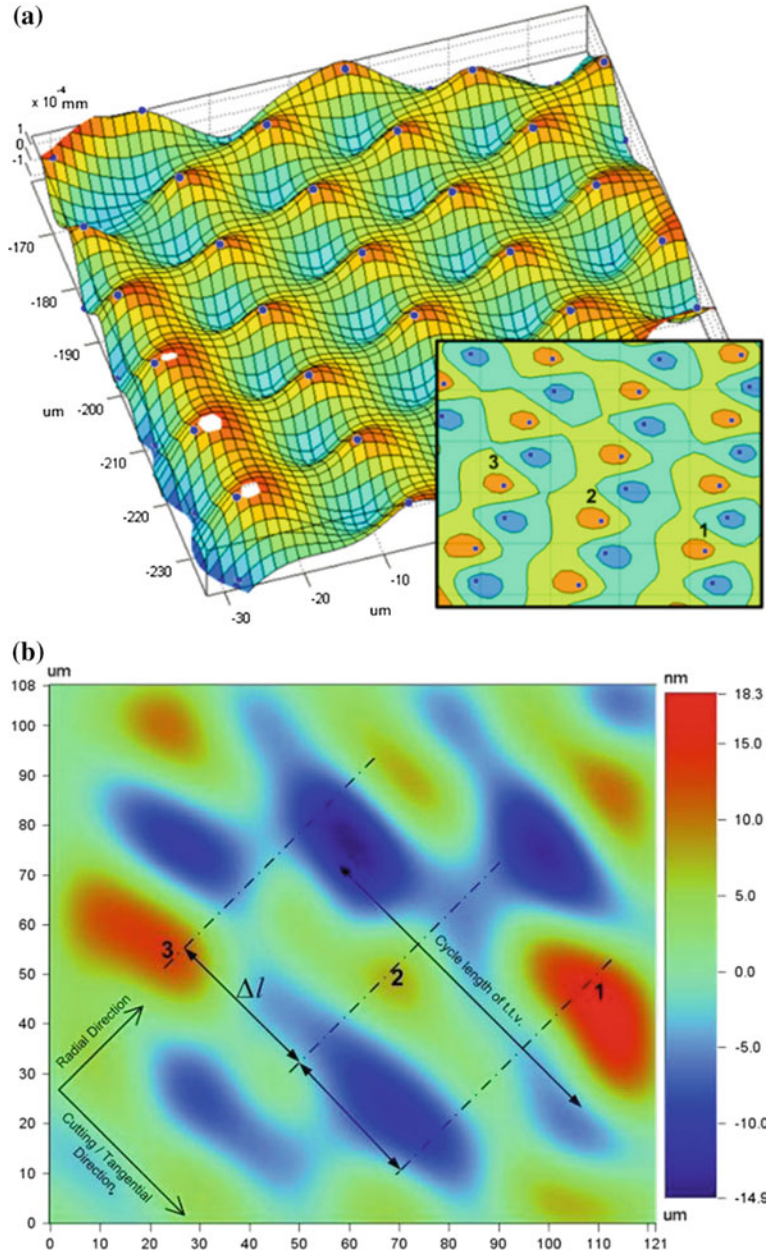

Fig. 9.21 **a** Simulated surface profile with tool-tip vibration and its *contour plot*; **b** corresponding measured surface profile and identified periodic fluctuations

The 3D data of the surface profile in Experiment 2 are recorded, and the noise information of the high spatial frequency and the frequency corresponding to $z_0(t)$ are eliminated by a band-pass filter to retain the key features of the machined surface. The peaks and valleys induced by tool-tip vibration are observed along the cutting direction. As indicated, the measured cycle length also agrees with Eq. (9.17). Three consecutive peak locations are labelled with numbers (1, 2 and 3) and three corresponding valleys are identified in the bottom right region. The simulated pattern (also labelled with 1, 2 and 3 in Fig. 9.21a) perfectly matches with that appearing on the measured pattern. This result further verifies both the theory and modelling of surface generation and the importance of tool-tip vibration. Therefore, the modelling of surface roughness should consider both the kinematic surface roughness and the surface roughness induced by tool-tip vibration.

9.5.2 *Formation of Spiral Marks on the Machined Surface*

An instant application of the proposed model of surface generation can be found to explain the formation of the spiral marks observed in the experiments, as shown in Fig. 9.17. In general, the formation of spiral marks is due to the existence of incomplete tool-tip vibration cycles in adjacent turning marks. The generic temporal relationship is expressed by Eq. (9.21), where S is the spindle speed (rpm), T_{spd} is the cycle time per revolution (s), T_{ttv} is the cycle time of tool-tip vibration, n is an integral number of complete cycles and Δt is the total remainder time besides n complete cycles in a single cycle T_{spd}. The superscripts (−) and (+) are employed to indicate that the source of the remainder time is from the previous revolution of the spindle cycle and the remainder time accumulates and is used for the next revolution of the spindle. The condition of Eq. (9.22) holds when the feed rate is low and a very small discrepancy exists for adjacent turning marks. Although unachievable in reality, the equality holds only when the surface (linear) speed is constant for adjacent turning marks. The remainder time Δt directly results in a position shift of peak (and valley) locations, as shown by the numbered peaks in Fig. 9.21b. The shift length Δl is a variable of distance to the centre D and Δt, and is obtained by Eq. (9.23). The consecutive shift of peaks forms the "spiral arms" observed in the overall situation.

$$T_{\text{spd}} = \frac{60}{S} = n \cdot T_{\text{ttv}} + \Delta t = \Delta t^{(-)} + n \cdot \frac{1}{f_{\text{ttv}}} + \Delta t^{(+)} \tag{9.21}$$

$$\Delta t^{(-)} + \Delta t^{(+)} \leq \frac{1}{f_{\text{ttv}}} \tag{9.22}$$

$$\Delta l = \frac{2\pi S}{60} \cdot D \cdot \Delta t \tag{9.23}$$

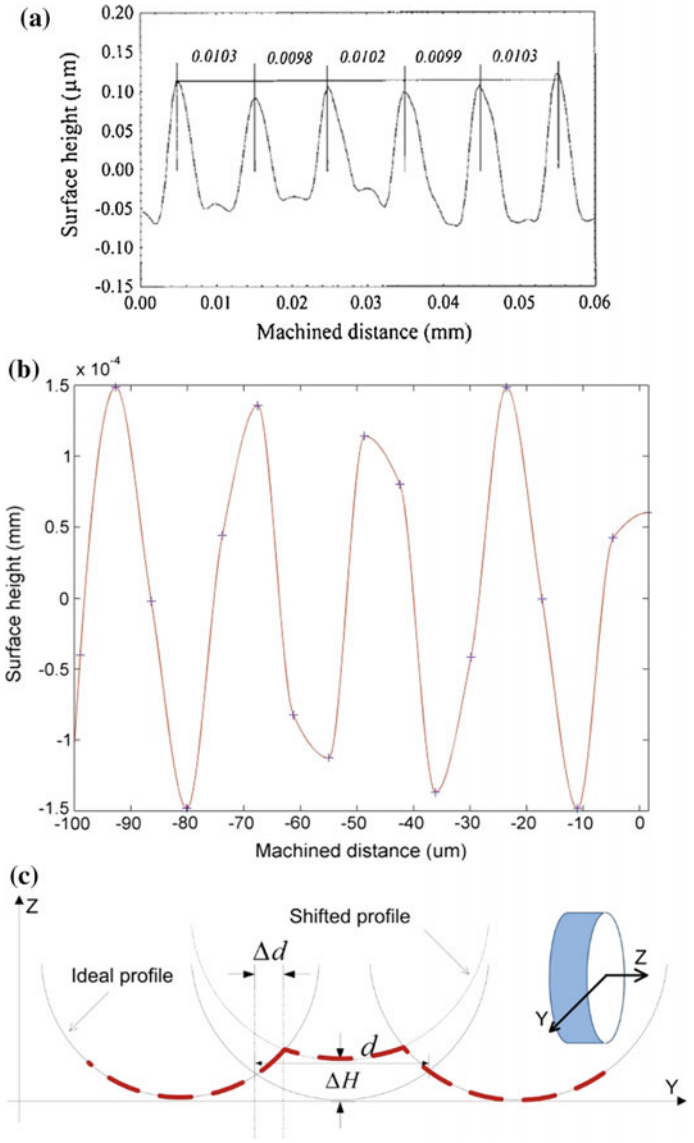

Fig. 9.22 **a** Successive turning marks on the measured radial profile by To et al. (2001); **b** simulated profile with the model of tool-tip vibration; **c** Schematic of shifted profile on the adjacent turning marks

9.5.3 Spatial Error on the Profile in the Feed Direction

To study the influence of material swelling on surface roughness, To et al. (2001) designed a series of face turning experiments on single crystal copper and aluminium workpieces and the machined surface was measured along the radial (feed) direction. At a constant spindle speed and feed rate, the peak-to-peak intervals measured on the surface profile along the feed direction should be equally spaced in an ideal case. However, in the experiments conducted by To et al. (2001), a spatial error was identified on the continuous three intervals on the radial measurement with a particular ratio, as in the normalised form in Eq. (9.24a), where $d_i^{(a)}$ denotes the distance of the ith (i = 1, 2 and 3) intervals in the subfigure (a). A radial profile extracted from the simulated data of the surface profile is shown in Fig. 9.22(b). The distance ratio of the predicted profile is expressed by Eq. (9.24b). A good correlation is found between the simulated and the measured data. A further explanation for the spatial error can be deduced from the schematic diagram in Fig. 9.22c. The successive three turning marks along the feed direction are plotted. Since the effect of tool-tip vibration on the machine surface is approximated by a sinusoidal wave, the ideal profile and shifted profile are indicated by arrows. Following the notation of Eq. (9.22), the shifted height on the surface profile (ΔH) can be expressed by Eq. (9.25), in which the time shift for the current turning mark $\left(\Delta t^{(-)}\right)$ is equal to the remainder time $\left(\Delta t^{(+)}\right)$ of the last turning mark at the same radial location.

$$d_1^{(a)}:d_2^{(a)}:d_3^{(a)} = 1{:}0.9515{:}0.9903 \tag{9.24a}$$

$$d_1^{(b)}:d_2^{(b)}:d_3^{(b)} = 1{:}0.7566{:}0.9996 \tag{9.24b}$$

$$\Delta H = A_{\mathrm{ttv}}\left[1 - \sin\left(2\pi\omega\Delta t^{(-)} + \phi_0\right)\right] \tag{9.25}$$

References

Abouelatta, O. B., & Mádl, J. (2001). Surface roughness prediction based on cutting parameters and tool vibrations in turning operations. *Journal of Materials Processing Technology, 118,* 269–277.

Bispink, T., & Weck, M. (1992). Performance analysis of feed-drive systems in diamond turning by machining specified test samples. *CIRP Annals - Manufacturing Technology 41*(1), 601–604.

Cheung, C. F., & Lee, W. B. (2000a). A multi-spectrum analysis of surface roughness formation in ultra-precision machining. *Precision Engineering, 24,* 77–87.

Cheung, C. F. & Lee, W. B. (2000b). A theoretical and experimental investigation of surface roughness formation in ultra-precision diamond turning, *International Journal of Machine Tools & Manufacture*, *40*, 979–1002.

Cheung, C. F., & Lee, W. B. (2001). Characterisation of nanosurface generation in single-point diamond turning. *International Journal of Machine Tools and Manufacture, 41,* 851–875.

Hocheng, H., & Heieh, M. L. (2004). Signal analysis of surface roughness in diamond turning of lens molds. *International Journal of Machine Tools and Manufacture, 44,* 1607–1618.

Jang, D. Y., Choi, Y.-G., Kim, H.-G., & Hsiao, A. (1996). Study of the correlation between surface roughness and cutting vibrations to develop an on-line roughness measuring technique in hard turning. *International Journal of Machine Tools and Manufacture, 36,* 453–464.

Kong, M. C., Lee, W. B., Cheung, C. F., & To, S. (2006). A study of materials swelling and recovery in single-point diamond turning of ductile materials. *Journal of Materials Processing Technology, 180*(1–3), 210–215.

Lee, W. B., & Cheung, C. F. (2001). A dynamic surface topography model for the prediction of nano-surface generation in ultra-precision machining. *International Journal of Mechanical Sciences, 43,* 961–991.

Li, L., Collins, S. A., Jr., & Yi, A. Y. (2010). Optical effects of surface finish by ultraprecision single point diamond machining. *Transactions of ASME, Journal of Manufacturing Science and Engineering, 132,* 021002-1–021002-9.

Piispanen, V. (1948). Theory of formation of metal chips. *Journal of Applied Physics, 19,* 876–881.

Recht, R.F. (1964), Catastrophic thermoplastic shear, Journal of Applied Mechanics, pp. 189–193.

Takasu, S., Masuda, M. & Nishiguchi, T. (1985). Influence of steady vibration with small amplitude upon surface roughness in diamond machining, *Annals of the CIRP*, *34*(1), 463.

To, S., Cheung, C. F., & Lee, W. B. (2001). Influence of material swelling on surface rough-ness in diamond turning of single crystals. *Materials Science and Technology, 17,* 102–108.

Wang, H., To, S., Cheung, C. F. & Lee, W. B. (2008). Finite element simulation of the cutting process in SPDT, *Proceedings of the International Conference of the EUSPEN*, *2*, 86–89.

Wang, H., To, S., Chan, C. Y., Cheung, C. F., & Lee, W. B. (2010). A theoretical and experimental investigation of the tool-tip vibration and its influence upon surface generation in single-point diamond turning. *International Journal of Machine Tools and Manufacture, 50,* 241–252.